Microbeam Radiation Therapy Opens a Several Days' Vessel Permeability Window for Small Molecules in Brain Tumor Vessels

Marine Potez, Claire Rome, Benjamin Lemasson, Pierre Heemeryck, Jean Albert Laissue, Vasile Stupar, Hervé Mathieu, Nora Collomb, Emmanuel L Barbier, Valentin Djonov, et al.

INTERNATIONAL JOURNAL OF
RADIATION ONCOLOGY • BIOLOGY • PHYSICS
www.redjournal.org

BIOLOGY CONTRIBUTION

Microbeam Radiation Therapy Opens a Several Days' Vessel Permeability Window for Small Molecules in Brain Tumor Vessels

Marine Potez, PhD,* Claire Rome, PhD,† Benjamin Lemasson, PhD,† Pierre Heemeryck, MS,‡ Jean Albert Laissue, Pr,§ Vasile Stupar, PhD,†,‖ Hervé Mathieu, PhD,†,‖ Nora Collomb, BS,‖ Emmanuel L. Barbier, PhD,†,‖ Valentin Djonov, Pr,* and Audrey Bouchet, PhD*,‡

*Institute of Anatomy, Group Topographic and Clinical Anatomy, University of Bern, Bern, Switzerland; †University Grenoble Alpes, Inserm U1216, Grenoble Institut Neurosciences, La Tronche, France; ‡Inserm U1296 "Radiation: Defense, Health, Environment," Lyon, France; §University of Bern, Bern, Switzerland; and ‖University Grenoble Alpes, Inserm, CNRS, CHU Grenoble Alpes, IRMaGe, Grenoble, France

Received Sep 4, 2023; Accepted for publication Feb 5, 2024

Purpose: Synchrotron microbeam radiation therapy (MRT), based on an inhomogeneous geometric and microscopic irradiation pattern of the tissues with high-dose and high-dose-rate x-rays, enhances the permeability of brain tumor vessels. This study attempted to determine the time and size range of the permeability window induced by MRT in the blood-brain (tumor) barrier.
Methods and Materials: Rats-bearing 9L gliomas were exposed to MRT, either unidirectional (tumor dose, 406 Gy) or bidirectional (crossfired) (2 × 203 Gy). We measured vessel permeability to molecules of 3 sizes (Gd-DOTA, Dotarem, 0.56 kDa; gadolinium-labeled albumin, ∼74 kDa; and gadolinium-labeled IgG, 160 kDa) by daily in vivo magnetic resonance imaging, from 1 day before to 10 days after irradiation.
Results: An equivalent tumor dose of bidirectional MRT delivered from 2 orthogonal directions increased tumor vessel permeability for the smallest molecule tested more effectively than unidirectional MRT. Bidirectional MRT also affected the permeability of normal contralateral vessels to a different extent than unidirectional MRT. Conversely, bidirectional MRT did not modify the permeability of normal or tumor vessels for both larger molecules (74 and 160 kDa).
Conclusions: High-dose bidirectional (cross-fired) MRT induced a significant increase in tumor vessel permeability for small molecules between the first and the seventh day after irradiation, whereas permeability of vessels in normal brain tissue remained stable. Such a permeability window could facilitate an efficient and safe delivery of intravenous small molecules (≤0.56 kDa) to tumoral tissues. A permeability window was not achieved by molecules larger than gado-grafted albumin (74 kDa). Vascular permeability for molecules between these 2 sizes has not been determined.

Corresponding authors: Emmanuel L. Barbier, PhD; and Audrey Bouchet, PhD; E-mail: emmanuel.barbier@univ-grenoble-alpes.fr, audrey.bouchet@inserm.fr

Disclosures: The Grenoble magnetic resonance imaging facility IRMaGe was partly funded by the French program "Investissement d'Avenirm," run by the 'Agence Nationale pour la Recherche,' through the grant 'Infrastructure d'avenir en Biologie Santé' (ANR-11-INBS-0006). The study was partially funded by the Bernische Krebsliga program, grant n.37223 (PI: AB), by the Fondation ARC (PI: AB); by the Ligue contre le cancer region Isère (PI: AB); and by the Oncostarter program from the Cancéroplôle Lyon Auvergne-Rhône-Alpes (PI: AB).

Data Sharing Statement: Research data are not available at this time.

Acknowledgments—We thank Hélène Bernard for her help in the early stages of the project. We also thank the staff of the GIN animal facility for their logistical support and for their assistance during the long working hours spent with the animals. Elke Bräuer-Krisch did so many things for this project. From the dose calculation, to support during the nights of irradiation at the synchrotron, we will remember her constant friendship throughout our years of collaboration. We miss her. Finally, we warmly thank Chantal Rémy for her invaluable support throughout the project (from the project design to data processing) and for her daily attention during the weeks and during the long MRI weekends. Wishing you a happy retirement!

https://doi.org/10.1016/j.ijrobp.2024.02.007

Introduction

Patients with high-grade gliomas have a particularly poor prognosis, associated with a median survival time of 16 months after glioblastoma diagnosis, despite improved current standard treatments.[1] Intratumoral distribution of therapeutic molecules to all tumor areas, adapted to physiooanatomic characteristics of solid tumors, limits the efficiency of multimodal therapies, especially of blood-borne chemotherapies.[2]

The challenge of drug delivery is tough for brain pathologies burdened with a blood-brain barrier (BBB), a highly selective physiological obstacle for molecules circulating in the blood.[3] Indeed, continuous tight interendothelial junctions, absence of transendothelial channels or pinocytotic vesicles, and the presence of active efflux transporters such as a specific carrier-mediated transport system in endothelial cells provide a high selectivity to this physiological barrier for crossing molecules.[3] The blood-brain tumor barrier (BBTB) retains characteristics of the BBB even when the integrity of the vascular wall in solid tumors is disturbed. As a result, the BBTB exhibits heterogeneous vascular permeability and perfusion, which contributes to suboptimal drug delivery to all tumor masses.[4-7] The extravasation of therapeutic molecules complicates the problem.

Different strategies can circumvent these limits.[4,5] Among them, conventional radiation therapy was reported as an efficient temporal disruptor of the BBTB.[8] In a clinical study, delivery of cumulative doses of 20 Gy in fractions of 2 Gy opened the BBTB and optimized the effects of intracranial chemotherapy.[9]

Since 2010, synchrotron microbeam radiation therapy (MRT) has been proposed as a strategy to specifically enhance tumor vessel permeability before drug administration.[10] MRT is based on an inhomogeneous geometric and microscopic irradiation pattern of the tissues, produced by a spatial and periodical alternation of the dose distribution. Technically, it is a spatial fractionation of incident, synchrotron-generated x-ray beams (characterized by low energy, high dose rate, and a negligible divergence) into arrays of multiple-parallel, micrometer-wide planar beamlets. Those beamlets deliver high ("peak") radiation doses (hGy) in their path; they are separated by wider "valleys" (up to few hundred microns), exposed to much lower doses. This irradiation has been developed since the 1990s as a new form of preclinical radiation therapy for brain tumors.[11] MRT efficiently controls the growth of different experimental tumor models, among them carcinomas, gliomas,[12-16] melanoma,[17] and even spontaneous canine brain tumors.[18] Despite a peak dose of several hundred gray in microbeam paths, the radiotolerance of normal tissues in the brains of rodents,[19-22] piglets,[23] duck embryos,[24] rat skin,[25] and in chick chorioallantoic membrane (CAM) was surprisingly high.[26] No changes in vascular morphology, density, or blood volume occurred in normal brain tissue after unidirectional MRT application of several hundred gray.[10,19,27] Even leakage and damage induced in normal vessels resolved few days in the path of a microbeam of 1000 Gy.[19] Conversely, MRT induced vascular damage of immature and tumoral vessels.[28] A combination of MRT and chemotherapy with a colchicine derivative (JAI-51) caused an increase in permeability of the BBTB in a glioma in vivo.[10] The survival time of the animals was significantly greater than that achieved by a uniform, homogenous synchrotron radiation therapy.[27,29] JAI-51 alone was not efficient.

At present, in a transplantable intracranial high-grade glioma (9L) in rats exposed to MRT, we characterized the time window of permeability to molecules of various sizes, in normal brain and in tumor vessels. We monitored daily in vivo the effects of 2 different configurations, unidirectional MRT or bidirectional (crossfired) MRT, using magnetic resonance imaging (MRI). In both configurations, MRT induced a significant increase in tumor vessel permeability: a temporal permeability window for the smaller molecule (0.56 kDa) persisted in the tumor at least 5 days after irradiation. Only after bidirectional (crossfired) MRT did this window, for that molecule, remain in place for at least 10 days. The molecular size influences the time window and the molecular delivery across an intact or disrupted BBBs and BBTBs.[30] Therefore, the role of MRT was tested for different sizes of molecules, ranging from that of nanoparticles to that of circulating proteins: both configurations of MRT failed to modify normal or tumor vessel permeability for the 2 biggest tested molecules (74 and 160 kDa).

Methods and Materials

Animals

All procedures related to animal care conformed to the Guidelines of the French Government with license 04598.01 and 045998.03, and to those issued by both the European Synchrotron Radiation Facility (ESRF) Internal Evaluation, and Grenoble Institute of Neurosciences (GIN) Committees for Animal Welfare and Rights. Charles River Laboratories in France supplied the rats for this study.

Figure 1 displays the number of animals and of acquisitions in vivo available at each time. T_n. stands for the number of days (n) elapsed since the irradiation.

The animals were housed in groups of 3 or 4 per cage, depending on their weight. The light cycle was nonreversed circadian, and the room temperature was 21 ± 1°C. An environmental enrichment of the cages allowed the rats to hide, gnaw, and bury objects.

After a short inhalation of isoflurane 5% in air, we maintained anesthesia by isoflurane 2.5% for tumor implantation, irradiation at ESRF, and MRI examination at GIN. Then, we adjusted it individually according to cardiopulmonary status, signs of overanesthesia, or of awakening of the rats.

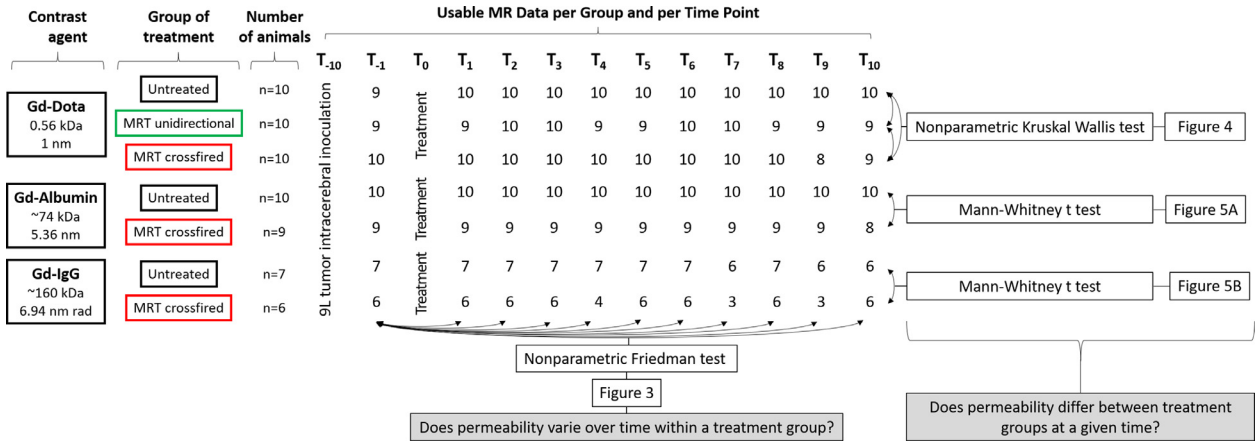

Fig. 1. Experimental design. Diagram representing each experimental step involving contrast agent, tumor inoculation, number of rats, and treatment group: unidirectional MRT (MRT uni, green), bidirectional (crossfired) MRT (MRT cross, red), and untreated (black). T_{day} expresses days after start of treatment, and N indicates number of animals with exploitable MRI data for each time and each treatment group. To evaluate the permeability compared with the day before irradiation, we used a nonparametric Friedman test followed by Dunn's multiple comparisons test. For the statistical comparison between the 3 groups, we used a nonparametric Kruskal-Wallis test followed by Dunn's multiple comparisons test for each time. A Mann-Whitney test compared nonparametric values of 2 different groups with Gd-albumin and Gd-IgG contrast agent. *Abbreviations*: MRI = magnetic resonance imaging; MRT = microbeam radiation therapy.

To alleviate postoperative craniotomy pain, we injected lurocaine (max 8 mg/kg) subcutaneously before surgery. We weighed the animals after tumor implantation and observed them at least once a day. We graded suffering according to an evaluation grid validated by the ethics committee of [anonymized], including signs and symptoms such as weight loss, hair maintenance, epistaxis, prostration, abnormal mobility, hypo- or akinesia, head tilt, and rotation of the animal. If alert criteria arose, we offered special food. The endpoint was set if no improvement occurred after 2 days, or if the animal's condition deteriorated rapidly. Inhalation of isoflurane 5% followed by an intracardial injection of Dolethal (250 mg/kg) led to their death.

At MRI acquisitions, we controlled the respiratory frequency, as well as the body temperature of the rats, by use of a heating pad during preparation, and then by adjustment with a bed heated with circulating water inside the MRI magnet.

Stereotaxic implantation of tumor cells

Ten days before irradiation (T_{-10}), anesthetized Fischer rats (n = 62), placed in a stereotactic head holder,[31] received an injection (Hamilton syringe) of 4.10^4 9L cells in 2.4 μL of Dulbecco's Modified Eagle Medium in their right caudate nucleus, at the level of the bregma. The site was 9 mm anterior to the ear-bars, 3.5 mm lateral from the bregma, and 5.5 mm deep from the skull surface.

Group sorting

All MRI data were acquired at 4.7T with a volume/surface cross coil configuration (Avance III console; Bruker – Grenoble MRI facility IRMaGE). Two days before starting the treatment ($T-_2$), we sorted the 62 rats for groups with similar mean tumor size for each experimental session, by anatomic MRI (T_2-weighted image).

To test permeability to Gd-DOTA molecule (Dotarem; Guerbet), we used 10 rats in each of the 3 groups: control group (untreated), unidirectional MRT group, and bidirectional (crossfired) MRT group.

To test permeability to the Gd-Alb molecule (Galbumin, gadolinium-labeled albumin; BioPhysics Assay Laboratory Inc), we used 10 rats in the control group and 9 rats in the bidirectional MRT group. To test permeability to the Gd-IgG molecule (Gd-IgG, gadolinium-labeled IgG; BioPhysics Assay Laboratory Inc), we used 7 rats in the control group and 6 rats in the bidirectional MRT group.

Synchrotron irradiation on T_0

The ID17 biomedical beamline at the (ESRF) uses x-rays emitted tangentially from relativistic electron bunches circulating in a storage ring. The wiggler produces a wide spectrum of photons that extends, after filtration, from 50 over 350 keV (median energy, 90 keV). The mean dose rate was ~13,000 Gy/s.[32] A multislit collimator shaped the beam into a quasilaminar array of rectangular, microscopically thin, and quasiparallel microbeams.[15] We calculated the doses by means of the Monte Carlo method normally used at (anonymized) for MRT dose planning and quality assurance.[33] The 3 sorted groups of rats are shown in Figure 1. For the MRT groups, the beam consisted of 10-mm-high arrays of 40 vertical, planar microbeams (50-μm width, 200-μm on-center spacing). Unidirectional MRT reached from the anatomically right side to the left. The peak

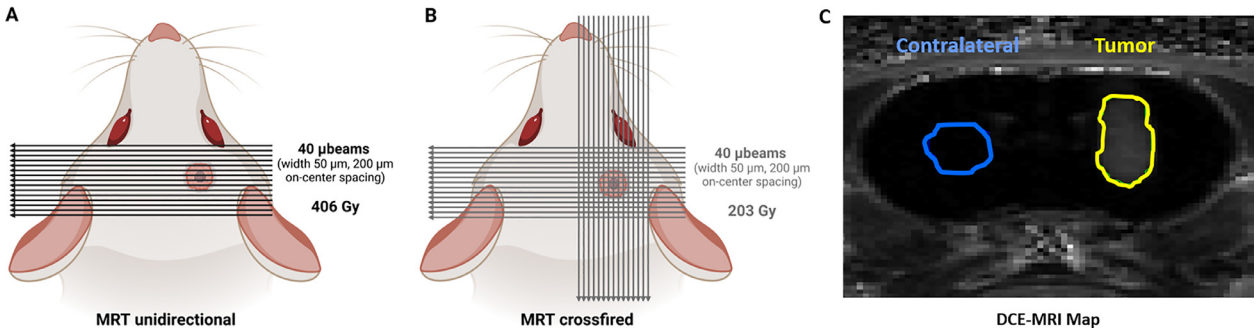

Fig. 2. Schematic representation of MRT irradiation geometry in intracranial glioma-bearing rats. The synchrotron beam was shaped into 10-mm-high arrays of 40 vertical, planar microbeams (5-μm width, 200-μm on-center spacing). (A) Unidirectional MRT was applied from the anatomically right side to the left with a peak entrance dose of 500 Gy. At tumor depth, peak and valley dose were 406 Gy and 17.7 Gy, respectively. (B) For bidirectional (crossfired) MRT, one array was anteroposterior, parasagittal, in the right hemisphere, the other array lateral. In unidirectional MRT, the array focused on the tumor sited in the anterior part of the right hemisphere; in bidirectional MRT, both arrays crossed orthogonally at the tumor site. Each array delivered 203.25 Gy in-microbeam tumor dose (250 Gy at entrance) and 8.8 Gy valley dose. (C) MRI DCE-enhancement map of 9L-bearing rat. Solid blue and yellow lines manually delineate the tumor and the contralateral region of interest, respectively. *Abbreviations*: DCE = dynamic contrast-enhanced; MRI = magnetic resonance imaging; MRT = microbeam radiation therapy.

entrance dose of 500 Gy corresponded to a peak and valley dose of 406 and 17.7 Gy, respectively, at tumor depth (Fig. 2A). Bidirectional (crossfired) MRT used 2 arrays, each similar to that of unidirectional MRT: one anteroposterior, the other lateral, both arrays intersecting orthogonally in the tumor sited in the anterior part of the right hemisphere. Each of the 2 arrays applied a 203.25-Gy in-microbeam tumor dose (250 Gy at entrance) and an 8.8-Gy valley dose (Fig. 2B).

In vivo MRI for vascular permeability monitoring

We imaged the 62 animals 1 day before (T_{-1}) treatment, then daily from 1 (T_1) to 10 days after treatment (T_{10}). After induction of anesthesia, a catheter inserted in the tail vein of the animal allowed for delivery of contrast. For the magnetic resonance (MR) sequences, we used the geometry of eleven 0.8-mm-thick slices, field of view: 30 × 30 mm, voxel size: 234 × 234 × 800 μm, as described.[27,34] We used anatomic T_2-weigthed images to visualize tumor mass and dynamic contrast-enhanced (DCE) MRI to assess vascular integrity. Multiple T_1-weighted images (n = 30, 30.4 seconds per image) were acquired with an accelerated spin-echo sequence (repetition time/echo time = 800/5.05 ms). After the acquisition of 4 baseline images, we administered a bolus of contrast agent through the tail vein in about 1 second and flushed with 250 μL of saline. Thereon we acquired 26 images.

Contrast agents were of 3 different sizes: (1) media gadolinium-1,4,7,10-tetraazacyclododecane-1,4,7,10-tetraacetic acid (Gd-DOTA, Dotarem, 200 μmol/kg [150.76 g/kg]) with a molecular weight of 0.56 kDa and a hydrodynamic diameter of 1 nm for the Gd-DOTA group; (2) gadolinium-labeled albumin (Gd-albumin, 160 mg/kg) with a molecular weight of ~74 kDa and a hydrodynamic diameter of ~5.4 nm for the Gd-albumin group; and (3) gadolinium-labeled IgG (Gd-IgG, 160 mg/kg) with a molecular weight of 160 kDa and a hydrodynamic diameter of ~6.9 nm for the Gd-IgG group.

For an enhancement map (DCE enhancement) we computed, pixel-wise, the relative signal enhancement between the mean MR signal across the 4 images received before the injection of the contrast agent and the peak MR signal measured after injection.

Data analysis

For image processing, we used the MATLAB 7 environment (MathWorks), with custom MP3 software,[35] freely available on GitHub (https://github.com/nifm-gin/MP3). We defined a tumor region of interest (ROI) by manually contouring the tumor on all on the T_2-weigthed images of MR slices on which the tumor was visible, as well as a ROI of similar size in the normal caudate nucleus area of the contralateral hemisphere. To export the individual contrast enhancement values, we reported tumor and contralateral ROI on DCE maps (Fig. 2C).

We excluded data altered by acquisition artifacts (eg, movement, sequence running errors) or by inadequate injection of contrast agents. Figure 1 shows the number of data sets fully exploited for analysis.

Statistical analysis

We calculated all statistical analyses and the area under the curve values with the GraphPad Prism program 8.2.0 version (GraphPad Software). To test and/or compare (1) the normality of the samples, we used the normality and log-normality tests; (2) nonparametric statistical methods for the analysis of non-Gaussian distribution of the data and n

values <30; and (3) for modifications in tumor and normal vessel permeability over time, we used the nonparametric Friedman test, wherein each row represented matched data. Each time point was compared with the day before treatment ($T-_1$). (4) To compare 3 or more paired groups, the Friedman test followed by Dunn's multiple comparisons test was used (Fig. 3). (5) To compare 3 unpaired groups at each time point for the Gd-DOTA molecule, a nonparametric Kruskal-Wallis test was used followed by Dunn's multiple comparisons test, to provide a reliable approach for detecting differences in permeability between treatment groups at various times (Fig. 4). (6) To compare nonparametric values of the 2 different groups tested in Figure 5, using Gd-albumin and Gd-IgG contrast agent, the Mann-Whitney *t* test for unpaired data was used. We considered values as significantly different when $P < .05$.

Figure 5C displays means ± SEMs of DCE rehaussement for the 11 time points observed in contralateral and tumor tissues in either untreated rats, or rats exposed to MRT, with Gd-DOTA injection (Fig. 4E), Gd-albumin injection (Fig. 5C), or Gd-IgG injection (Fig. 5D). DCE-rehauss = relative signal enhancement between the mean MR signal across the 4 images obtained before the injection of contrast agent and the peak MR signal measured after injection (in %)

Results

MRT effectively increases the permeability of brain tumor vessels for small molecules

Untreated tumors (Fig. 3A, right panel), had a stable vascular permeability during the 12 observation days. A significant increase occurred at T_8 only (136.1% of increase, T_8 vs T_{-1}: $P = .0374$).

Unidirectional MRT (Fig. 3B, right panel) induced a significant increase of the blood tumor vessel permeability to Gd-DOTA, compared with the $T_{-1\ value}$, from the first day after irradiation to T_8 ($P < .005$), except at T_2 ($P = .21$). The maximum permeability increase occurred on T_5 (193.7% of increase, T_5 vs T_{-1}: $P < .0001$).

Bidirectional (crossfired MRT) induced an increase in tumor permeability that started to be significant from T_3 to T_{10}, compared with the $T_{-1\ value}$ ($P < .05$ for T_3 and $P < .001$ for the other time points), except at T_9 ($P = .057$) (Fig. 3C, right panel). The peak increase in permeability occurred on T_6 (216% of increase, T_6 vs T_{-1}: $P < .0001$).

MRT modulates vascular permeability in normal brain tissue, depending on the dose

In the contralateral area of untreated rats (Fig. 3A, right panel), the permeability of normal brain vessels was not significantly modified compared with the day before irradiation (T_{-1}).

In the unidirectional MRT group (Fig. 3B, right panel), the vascular permeability in the contralateral area increased significantly, from the second day post irradiation (T_2) to T_8, in comparison with T_{-1}.

Conversely, in the contralateral area of the brain crossirradiated by bidirectional MRT (Fig. 3C, right panel), the vascular permeability increased significantly only from the 5th to the 10th day after irradiation ($P = .0301$ at T_5, $P < .0005$ at T_6, $P < .0001$ at T_7, T_8, T_9, and T_{10}) compared with T_{-1}.

MRT induces a permeability window suitable for small molecules

In tumors, there was no significant difference between the vessel permeability to Gd-DOTA after bidirectional (crossfired) and unidirectional MRT, during the whole experiment (Fig. 4A, B). Only bidirectional MRT induced a significantly greater value in tumors compared with untreated tissues ($P < .001$; Fig. 4A). Both MRT conformations increased the vascular permeability of the tumor versus that measured in the untreated group. In the unidirectional MRT group, the vessel permeability was significantly greater from the first day (T_1, $P = .0026$) to 5 days after irradiation only (T_5, $P = .0059$). In the bidirectional MRT group, the vessel permeability was significantly greater from the first day (T_1, $P = .0016$) to the last observed day post irradiation (T_{10}, $P = .0002$) (Fig. 4B).

In contralateral areas, in the whole experiment, the vessel permeability after unidirectional MRT was greater than the permeability after bidirectional MRT ($P = .0332$) and greater than the permeability in the untreated group ($P < .0001$) (Fig. 4C). The permeability of normal vessels was significantly greater in the unidirectional MRT group, from T_5 to $T_{10,}$ and in the bidirectional MRT group from T_1 to T_{10}, compared with that of the untreated group (Fig. 4D). In addition, the vessel permeability in the contralateral area was significantly greater from the first (T_1) to the sixth days (T_6) after unidirectional MRT in comparison with bidirectional MRT (Fig. 4D).

By comparing the temporal permeability between the treated and untreated group, time by time, we observed that (1) after unidirectional MRT, when the permeability was significantly greater in tumor vessels, the permeability was also greater in contralateral vessels. (2) After bidirectional MRT, there was a window between T_1 and $T_{4,}$ during which permeability to Gd-DOTA was significantly greater in the tumor but not in the contralateral area (Fig. 4B, D).

MRT does not induce an increase in vascular permeability for large molecules Gd-Alb and Gd-IgG

To test MRT for the induction of a tumor vessel permeability to protein-sized molecules, we used 2 contrast agents, Gd-Alb (~74 kDa) and Gd-IgG (~160 kDa). After

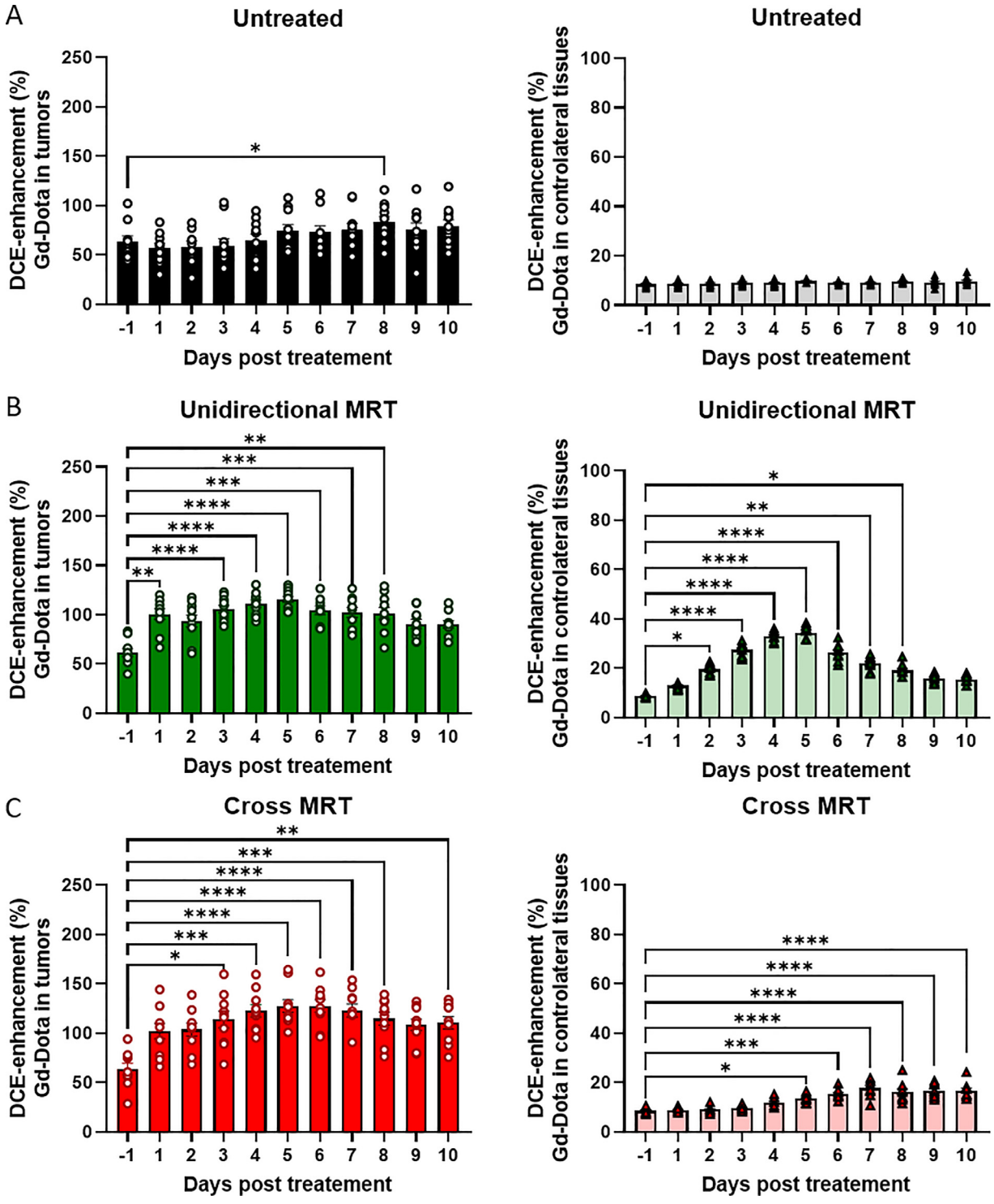

Fig. 3. Evolution of vascular permeability for the small molecule (Gd-DOTA, 0.56 kDa) in tumors and contralateral tissues after MRT. (A-C) Dynamic contrast enhancement (DCE) after Gd-DOTA injection, measured by magnetic resonance imaging (MRI) in 9L tumor (left panel) and normal brain tissue in the contralateral area (right panels) 1 day before to 10 days after irradiation. Black: (A) No treatment. Green: (B), unidirectional MRT. Red: (C) bidirectional ("cross") MRT. Individual values and mean ± SEM for each time are shown and compared with the permeability measured the day before the start of treatment ($T-_1$). Days exhibiting a significant difference from $T-_1$ are marked with asterisks, based on results of the statistical analysis conducted using the Friedman nonparametric test. *$P < .05$; **$P < .01$; ***$P < .001$; ****$P < .0001$. *Abbreviations*: MRI = magnetic resonance imaging; MRT = microbeam radiation therapy.

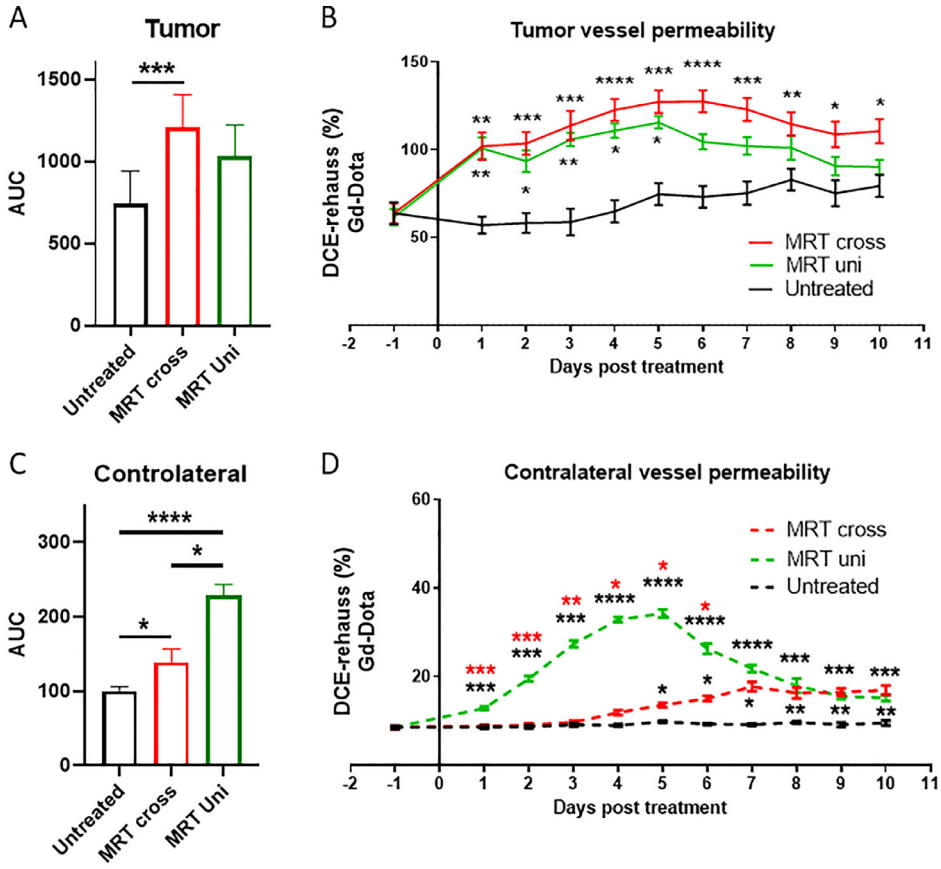

E	Percentage of DCE-rehaussement after Gd-Dota injection					
	Contralateral (mean ±SEM)			Tumor (mean ±SEM)		
	Untreated	MRT Unidir	MRT Cross	Untreated	MRT Unidir	MRT Cross
T-1	8.6 ±0.4	8.6 ±0.2	8.6 ±0.4	63.8 ±6.3	61.6 ±4.6	63.7 ±5.8
T1	8.6 ±0.4	13.0 ±0.4	8.9 ±0.3	57.0 ±4.8	100.7±6.1	102.0±7.8
T2	8.7 ±0.4	19.5 ±0.6	9.1 ±0.4	58.3 ±5.6	93.4 ±6.1	103.6±6.6
T3	9.2 ±0.4	27.4 ±0.8	9.7 ±0.3	58.7 ±7.6	105.8±3.7	113.8±8.4
T4	9.0 ±0.3	33.0 ±0.6	12.0 ±0.6	64.8 ±6.4	110.9±4.1	122.7±6.3
T5	9.8 ±0.2	34.3 ±0.9	13.6 ±0.5	74.6 ±6.3	115.5±3.5	127.4±6.5
T6	9.3 ±0.2	26.4 ±1.1	15.1 ±0.6	73.1 ±6.2	104.5±4.4	127.5±6.3
T7	9.2 ±0.3	21.8 ±0.8	17.8 ±1.1	75.3 ±6.7	102.1±5.1	123.0±6.6
T8	9.7 ±0.3	18.0 ±1.6	16.3 ±1.2	82.9 ±6.2	101.1±6.8	114.6±6.6
T9	9.2 ±0,5	15.6 ±0.6	16.5 ±0.8	75.1 ±7.3	90.6 ±5.2	108.±7.3
T10	9.6 ±0.6	15.2 ±0.7	17.0 ±1.1	79.4 ±6.3	90.1±4.1	110.5±7.0

****	***	**	*	Ns	*	**	***	****
Effects to avoid					Desired effects			

Fig. 4. Comparison of vascular permeability to small molecule (Gd-DOTA, 0.56 kDa) after MRT. Daily values of dynamic contrast enhancement (DCE) after Gd-DOTA (Dotarem) injection measured by MRI, in 9L tumor (A, B) and in normal brain tissue of the contralateral area (C, D). After unidirectional MRT (green), bidirectional MRT (red), no treatment (black). (A, C) Cumulative measurement of DCE in the tumor from $T-_1$ to T_{10} (A) or contralateral area (C) represented as total area under the curve (AUC). (B, D) Comparison of daily mean DCE measured 1 day before irradiation ($T-_1$) and until 10 days (T_{10}) after treatment in tumor (B), and in the contralateral area (D). Black asterisk: comparison with untreated group, red asterisk:

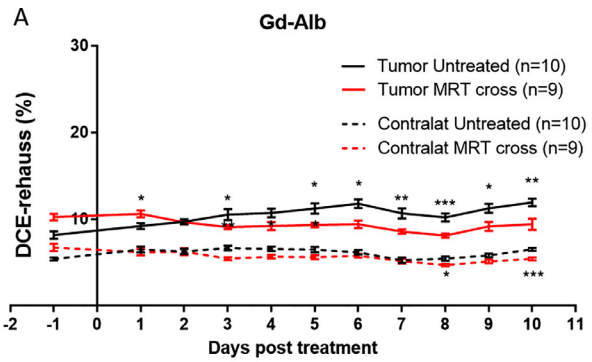

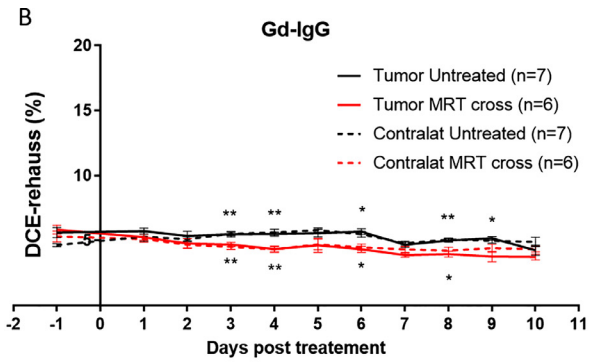

C

		Percentage of DCE-rehaussement after Gd-Albumin injection										
		T-1	T1	T2	T3	T4	T5	T6	T7	T8	T9	T10
Untreated	Contralateral (mean ±SEM)	5.4 ±1.7	6.5 ±0.3	6.3 ±0.3	6.7 ±0.3	6.6 ±0.2	6.5 ±0.3	6.2 ±0.3	5.3 ±0.3	5.4 ±0.3	5.8 ±0.2	6.5 ±0.2
	Tumor (mean ±SEM)	8.2 ±0.5	9.2 ±0.3	9.7 ±0.3	10.5 ±0.6	10.7 ±0.5	11.2 ±0.6	11.8 ±0.5	10.6 ±0.6	10.2 ±0.5	11.2 ±0.5	11.9 ±0.4
MRT Cross	Contralateral (mean ±SEM)	6.7 ±0.4	6.2 ±0.4	6.2 ±0.4	5.4 ±0.2	5.7 ±0.2	5.6 ±0.2	5.8 ±0.2	5.2 ±0.3	4.7 ±0.2	5.1 ±0.2	5.4 ±0.2
	Tumor (mean ±SEM)	10.2 ±0.4	10.6 ±0.4	9.6 ±0.2	9.1 ±0.2	9.2 ±0.5	9.3 ±0.3	9.4 ±0.5	8.2 ±0.3	7.5 ±0.3	9.2 ±0.5	8.7 ±0.7

D

		Percentage of DCE-rehaussement after Gd-IgG injection										
		T-1	T1	T2	T3	T4	T5	T6	T7	T8	T9	T10
Untreated	Contralateral (mean ±SEM)	4.7 ±0.1	5.3 ±0.4	5.1 ±0.2	5.5 ±0.1	5.6 ±0.3	5.8 ±0.2	5.5 ±0.2	4.8 ±0.2	5.1 ±0.1	5.0 ±0.2	4.9 ±0.4
	Tumor (mean ±SEM)	5.6 ±0.4	5.7 ±0.2	5.4 ±0.4	5.5 ±0.2	5.5 ±0.2	5.6 ±0.3	5.7 ±0.2	4.7 ±0.2	5.0 ±0.1	5.2 ±0.2	4.3 ±0.4
MRT Cross	Contralateral (mean ±SEM)	5.3 ±0.4	5.1 ±0.2	4.7 ±0.3	4.5 ±0.2	4.3 ±0.2	4.7 ±0.4	4.5 ±0.3	4.3 ±0.2	4.2 ±0.3	4.4 ±0.3	4.3 ±0.2
	Tumor (mean ±SEM)	5.8 ±0.3	5.3 ±0.2	4.8 ±0.4	4.7 ±0.2	4.4 ±0.2	4.6 ±0.5	4.3 ±0.2	3.9 ±0.2	4.0 ±0.2	3.8 ±0.4	3.7 ±0.2

Fig. 5. Vessel permeability to Gd-Alb (~74 kDa) and Gd-IgG (~160 kDa). Dynamic contrast enhancement (DCE) with Gd-Alb (A) and Gd-IgG injection (B) measured daily by MRI in 9L tumors (solid lines) and normal contralateral brain (dashed lines) 1 day before and until 10 days after bidirectional (cross-irradiation) MRT (red). Untreated animals (black). The asterisks above the upper curve indicate comparisons between untreated tumors and cross-irradiated tumors, determined through the Mann-Whitney *U* test. The asterisks below the lower curve show the comparisons between untreated contralateral tissue and cross-irradiated contralateral tissue. Mean ± SEM; $^{*}P < .05$; $^{**}P < .01$; $^{***}P < .001$. (C, D) Tables summarizing the mean and SEM values of the percentage of DCE rehaussement after injections of Gd-albumin (C) and Gd-IgG (D), 1 day and during the 10 days after the start of treatment for the untreated and bidirectional MRT groups. *Abbreviation*: MRT = microbeam radiation therapy.

bidirectional MRT, neither the tumors nor the contralateral tissue showed an increased permeability for both contrast agents at any time, compared with values in the nonirradiated group (Fig. 5A, B).

Discussion

The failure of chemotherapeutic molecules to gain access to tumor tissues remains a clear obstacle for successful combined treatments of cerebral tumors.[2] MRT, known to increase the permeability of brain tumor vessels,[10,27,28,36,37] has thus increased the efficacy of a preclinical chemotherapy of rats bearing high-grade brain tumors.[29] Further, a previous study conducted in F98 rat glioblastoma has shown that increased vascular permeability of a tumor due to MRT is (1) significantly greater and (2) earlier and more prolonged than that induced by homogeneous x-ray irradiation because it also affects particularly highly proliferative tumor areas. (3) Moreover, it targets all tumor areas that have different physiological characteristics, including those areas that are not affected by homogeneous irradiation.[27] MRT therefore appears to be a more effective treatment than homogeneous radiation therapy for tumors with heterogeneous tissues, such as high-grade gliomas.

Consequently, to find access to more efficient and safer therapeutic combinations, it was essential to characterize the effects of MRT on the vascular permeability of normal and tumoral brain tissues. The primary aim of the current study was to find the most appropriate time window for the injection of therapeutic molecules after MRT. This window will depend on the evolution of the vascular permeability in tumoral and normal brain tissues. Thus, we (1) measured the permeability in both tumor and normal brain tissues after exposure to 2 different configurations of MRT, each one delivering an equivalent dose to the tumor, but a different dose to normal tissues; (2) searched for the most appropriate MRT configuration that induced a vessel permeability window suitable for the administration of small molecules to the tumor but that would not endanger normal brain tissue; and (3) tested the capability of MRT to increase vascular permeability for large molecules such as albumin and

comparison with bidirectional MRT group. Mean ± SEM; $^{*}P < .05$; $^{**}P < .01$; $^{***}P < .001$ $^{****}P < .0001$. (E) Table summarizing the mean and SEM values of DCE rehaussement after Dotarem (Gd-DOTA) injection, 1 to 10 days after the start of treatment by unidirectional and bidirectional MRT, and in the untreated group. Significance between treated and untreated groups at each time shown by a color scale for effects to be avoided (gray) in normal tissue and for desired effects (yellow) in tumor tissue. *Abbreviations*: MRI = magnetic resonance imaging; MRT = microbeam radiation therapy.

IgG. A daily monitoring of DCE by in vivo MRI of rats with intracerebral high-grade 9L glioma reliably mirrored the vascular permeability.

While applying the same dose to the tumor (406 Gy by unidirectional irradiation or 2 × 203 Gy bidirectionally), the 2 conformations of MRT induced different responses of the blood tumor vessels (Figs. 3 and 4A, B). Differential effects caused by multiplication of direction of MRT by using more entrance ports, while delivering a constant dose to the tumor, was recently described in a histologic study focusing on cell death, vascular damage, and inflammatory responses.[38] In analogy, our in vivo MRI study did also indicate that tumor vascular permeability may depend on the number of MRT ports in uni- or bidirectional MRT. Both conformations significantly increased tumor permeability to a small molecule (Dotarem, 0.56 kDa) after irradiation (Fig. 3). However, only bidirectional MRT led most effectively to a significantly greater tumor vascular permeability, from 1 to 10 days postirradiation, versus values measured in untreated tumors (Fig. 4A, B). In a previous study,[38] an increased number of MRT ports was shown to delay tumor growth and improve survival. However, 7 days after delivering microbeams from 5 directions, the vascular blood volume of the tumor was lower than that of control animals; this reduction did not occur when microbeams originated from 2 directions only.[38]

Contralateral normal tissues area received only one direction of irradiation in both MRT configurations. Not surprisingly, the dose delivered by unidirectional MRT, twice as high as that of a single array in bidirectional MRT, induced a significantly greater vascular permeability in normal tissues (Fig. 4C, $P < .0001$). The kinetics of permeability in the contralateral tissue also differed between the 2 configurations. Although in the bidirectional MRT group, vascular permeability increased only from the fifth day after irradiation, it rose from the first day in the unidirectional MRT group (Fig. 3C). In contralateral normal tissues of the unidirectional MRT group exposed to 406 Gy, the vascular permeability was significantly greater from day 1 to 6 postradiation compared with that in the bidirectional MRT group exposed to 203 Gy. In the untreated group the permeability increased from day 1 to 10 (Fig. 4D). The dose received by the normal contralateral brain tissue at the passage of the microbeams during both MRT configurations was far superior to the dose that is known to induce dysfunction and death of endothelial cells.[39] We therefore suspect that the different effects observed in the vascular permeability of normal tissues relate to the valley dose received by the tissues sited between the microbeams. Such a permeability increase in normal tissues could be exploited to improve their supply of chemotherapeutic molecules. However, this valley dose should be kept as low as possible to avoid normal brain tissue toxicity.

It is important to avoid shortcuts when interpreting the effect of MRT on the permeability of normal vessels. Previous studies have concluded that MRT either does or does not modify the vascular permeability of normal brain tissue. These contrasting conclusions depend mainly on the different size of tested molecules, but also on the specifications of MRT, such as dose, width of microbeams, or number of ports. Serduc et al[19] detected no leakage of intravascular FITC-dextran (70 kDa) from 12 hours to 1 month after MRT using 25-μm-wide beams that delivered 312 or 1000 Gy to mice. Conversely, sulforhodamine B (0.58 kDa) did diffuse through the vessels. An MRT follow-up study[10] showed no change in the vascular permeability of normal rat brain tissue between 2 and 45 days after exposure to a unidirectional dose of 400 Gy delivered by 25-μm-wide microbeams; the test substance was a Gd-based contrast agent of 3.5 kDa.[10] However, 45 days after MRT, slight changes were observed in normal perilesional brain tissues of these rats exposed to 2 × 400 Gy by microbeams crossing from 2 directions.[10] By contrast, after unidirectional irradiation of rat brains with 50-μm-wide microbeams delivering 241 Gy, an MRI study using a 0.56-kDa contrast agent showed no significant change of normal vascular permeability. Transient changes occurred in the perilesional zone exposed to 2 directions of irradiation.[27] Multiplying the number of MRT directions while maintaining a constant dose to the target point increases the total volume of normal tissue exposed to radiotoxicity. However, a numerical increase of ports for incident MRT significantly enhanced tumor control and exponentially improved survival times of rats bearing tumors but did not modify their motor coordination nor their memory.[38] Even when weighing the effect of potential radiotoxic limitation, bidirectional (crossed) irradiation proved more effective in increasing permeability to small molecules in the tumor while minimally increasing vascular permeability and potentially damaging normal brain tissue. Further, the resulting time window from day 1 to day 4 after irradiation warranted (1) a tumor permeability that is significantly greater than in the untreated group and (2) a vascular permeability of the control tissue similar to that of the untreated group. There was only a small difference in the vascular permeability of contralateral tissue between the fifth and seventh day ($P = .032$), synchronous with that of the maximal tumor permeability ($P < .0001$). Therefore, we propose to use a window of permeability for small molecules comprised between the first and the seventh day after bidirectional MRT. Unidirectional MRT does not result in a time window in which the vascular permeability in the tumor is greater than that in untreated tumors (Fig. 4B).

An experiment in 2010 used the 9L glioma model in rats to show morphologic and permeability changes in irradiated vessels after MRT.[10] Observation times were 2, 5, and 8 days after irradiation; the entrance dose of bidirectional MRT was 2 × 400 Gy; the maximum permeability in the tumor occurred at 5 days after irradiation, characteristics similar to those made in the present study. In 2010, immunostaining of histologic tissue sections revealed an endothelial denudation of the tumor blood vessels from 2 days after irradiation[10,40] that remodeled blood vessels in the tumor. Consequently, collagen IV tubes partly supplied the tumor

with blood and probably increased the permeability. The preferential effect of MRT on tumor endothelial cells versus normal endothelial cells, that is, on cells in immature versus mature vessels, has been well described.[28] Previous research in CAMs demonstrated an increase in permeability to 70 kDa dextran as early as 45 minutes after MRT.[37] In the present study, an evaluation of the permeability by MRI within 45 minutes after irradiation was not possible because of technical constraints. However, we observed no increase in permeability to Gd-DOTA in the 3 animals imaged 2.5 hours after bidirectional MRT (*t* test: $P = .2168$, data not shown), although the microenvironment of orthotopic gliomas is not the same as that of CAMs.

To cross the BBB and BBTB, molecules must have an optimal size, charge, and physicochemical property. Protein and monoclonal antibodies are too large or have too hydrophilic characteristics to cross BBB, and especially tight junctions.[41] That makes it difficult to reach the core of brain tumors. Conversely, irinotecan (586 Da[42]) and temozolomide (194.15 Da[43]), which is the standard first-line treatment regimen for gliomas,[44] both cross the BBB and BBTB. Bidirectional MRT did not significantly increase the vascular permeability for larger molecules such as Gd-albumin (Gd-Alb, 74 kDa) or Gd-immunoglobulin (Gd-IgG, 160 kDa) (Fig. 5). The increase of signals measured was low, whatever the treatment group, as were the sporadic differences obtained between the groups. These results suggest for the first time that MRT does not improve the passage of large molecules (at least equivalent to 74 kDa) in normal and neoplastic brain tissues.

The permeability of tumor vessels induced by MRT can be exploited by coupling large with small molecules, for instance JAI-51, a synthesized small chemotherapeutic agent weighing 351.4 Da,[45] and meloxicam, a 351.40 Da[46] nonsteroidal anti-inflammatory drug. Although neither of these molecules alone modified animal survival, a supra-additive effect of a combined treatment occurred.[29,47]

Conclusion

We characterized the kinetics of vascular permeability induced in tumor and normal tissues by MRT, tracking results of serial in vivo MR images of 9L glioma-bearing rats. With an equal dose to the tumor, bidirectional MRT was more efficient than unidirectional MRT for the induction of permeability in tumor and harmless for normal tissues. We suggest that a permeability time window for molecules as large as 0.56 kDa, opening between the first and the seventh day after bidirectional MRT, facilitates an efficient and safe delivery of intravenously injected small molecules to tumoral tissues. Such a window was no longer achievable for molecules beyond the size of gado-grafted albumin (74 kDa). The use of gadolinium-labeled contrast agents with weights between Gd-DOTA (0.56 kDa) and Gd-albumin (74 kDa) might lead to a more precise measurement of the permeability window. A future description of the cellular and subcellular morphologic changes associated with permeability changes observed in vivo may clarify underlying mechanisms and optimize the choice of substances most suitable for therapeutic coupling with MRT.

References

1. Stupp R, Hegi ME, Gilbert MR, et al. Chemoradiotherapy in malignant glioma: Standard of care and future directions. *J Clin Oncol* 2007;25:4127-4136.
2. Holback H, Yeo Y. Intratumoral drug delivery with nanoparticulate carriers. *Pharm Res* 2011;28:1819-1830.
3. Pollay M, Roberts PA. Blood-brain barrier: A definition of normal and altered function. *Neurosurgery* 1980;6:675-685.
4. Marcucci F, Corti A, Ferreri AJM. Breaching the blood-brain tumor barrier for tumor therapy. *Cancers (Basel)* 2021;13:2391.
5. Wang D, Wang C, Wang L, et al. A comprehensive review in improving delivery of small-molecule chemotherapeutic agents overcoming the blood-brain/brain tumor barriers for glioblastoma treatment. *Drug Deliv* 2019;26:551-565.
6. Van Tellingen O, Yetkin-Arik B, De Gooijer MC, et al. Overcoming the blood-brain tumor barrier for effective glioblastoma treatment. *Drug Resist Updat* 2015;19:1-12.
7. Arvanitis CD, Ferraro GB, Jain RK. The blood−brain barrier and blood−tumour barrier in brain tumours and metastases. *Nat Rev Cancer* 2020;20:26-41.
8. van Vulpen M, Kal HB, Taphoorn MJB, et al. Changes in blood−brain barrier permeability induced by radiotherapy: Implications for timing of chemotherapy? (Review). *Oncol Rep* 2002;9:683-688.
9. Qin D, Ou G, Mo H, et al. Improved efficacy of chemotherapy for glioblastoma by radiation-induced opening of blood-brain barrier: Clinical results. *Int J Radiat Oncol Biol Phys* 2001;51:959-962.
10. Bouchet A, Lemasson B, Leduc G, et al. Preferential effect of synchrotron microbeam radiation therapy on intracerebral 9L gliosarcoma vascular networks. *Int J Radiat Oncol Biol Phys* 2010;78:1503-1512.
11. Brauer-Krisch E, Serduc R, Siegbahn EA, et al. Effects of pulsed, spatially fractionated, microscopic synchrotron x-ray beams on normal and tumoral brain tissue. *Mutat Res* 2010;704:160-166.
12. Bouchet A, Sakakini N, El Atifi M, et al. Early gene expression analysis in 9L orthotopic tumor-bearing rats identifies immune modulation in molecular response to synchrotron microbeam radiation therapy. *PLoS One* 2013;8:e81874.
13. Bouchet A, Sakakini N, El Atifi M, et al. Identification of AREG and PLK1 pathway modulation as a potential key of the response of intracranial 9L tumor to microbeam radiation therapy. *Int J Cancer* 2015;136:2705-2716.
14. Bouchet A, Bräuer-Krisch E, Prezado Y, et al. Better efficacy of synchrotron spatially microfractionated radiation therapy than uniform radiation therapy on glioma. *Int J Radiat Oncol Biol Phys* 2016;95:1485-1494.
15. Bräuer-Krisch E, Requardt H, Brochard T, et al. New technology enables high precision multislit collimators for microbeam radiation therapy. *Rev Sci Instrum* 2009;80 074301.
16. Serduc R, Bouchet A. MRT-boost as the last fraction may be the most efficient irradiation schedule for increased survival times in a rat glioma model. *J Synchrotron Radiat* 2023;30:591-595.
17. Potez M, Fernandez-Palomo C, Bouchet A, et al. Synchrotron microbeam radiation therapy as a new approach for the treatment of radioresistant melanoma: Potential underlying mechanisms. *Int J Radiat Oncol Biol Phys* 2019;105:1126-1136.
18. Adam JF, Balosso J, Bayat S, et al. Toward neuro-oncologic clinical trials of high-dose-rate synchrotron microbeam radiation therapy: First treatment of a spontaneous canine brain tumor. *Int J Radiat Oncol Biol Phys* 2022;113:967-973.

19. Serduc R, Verant P, Vial JC, et al. In vivo two-photon microscopy study of short-term effects of microbeam irradiation on normal mouse brain microvasculature. *Int J Radiat Oncol Biol Phys* 2006;64:1519-1527.
20. Serduc R, Christen T, Laissue J, et al. Brain tumor vessel response to synchrotron microbeam radiation therapy: A short-term in vivo study. *Phys Med Biol* 2008;53:3609-3622.
21. Slatkin DN, Spanne P, Dilmanian FA, et al. Subacute neuropathological effects of microplanar beams of x-rays from a synchrotron wiggler. *Proc Natl Acad Sci USA* 1995;92:8783-8787.
22. Laissue JA, Geiser G, Spanne PO, et al. Neuropathology of ablation of rat gliosarcomas and contiguous brain tissues using a microplanar beam of synchrotron-wiggler-generated X rays. *Int J Cancer* 1998;78:654-660.
23. Laissue JA, Blattmann H, Di Michiel M, et al. The weaning piglet cerebellum: A surrogate for tolerance to MRT (microbeam radiation therapy) in paediatric neuro-oncology. *Proc SPIE* 2001;4508:65-73.
24. Dilmanian FA, Morris GM, Le Duc G, et al. Response of avian embryonic brain to spatially segmented x-ray microbeams. *Cell Mol Biol (Noisy-le-grand)* 2001;47:485-493.
25. Zhong N, Morris GM, Bacarian T, et al. Response of rat skin to high-dose unidirectional x-ray microbeams: A histological study. *Radiat Res* 2003;160:133-142.
26. Sabatasso S, Laissue JA, Hlushchuk R, et al. Microbeam radiation-induced tissue damage depends on the stage of vascular maturation. *Int J Radiat Oncol Biol Phys* 2011;80:1522-1532.
27. Bouchet A, Potez M, Coquery N, et al. Permeability of brain tumor vessels induced by uniform or spatially microfractionated synchrotron radiation therapies. *Int J Radiat Oncol Biol Phys* 2017;98.
28. Bouchet A, Serduc R, Laissue JA, et al. Effects of microbeam radiation therapy on normal and tumoral blood vessels. *Phys Med* 2015;31:634-641.
29. Bouchet A, Boumendjel A, Khalil E, et al. Chalcone JAI-51 improves efficacy of synchrotron microbeam radiation therapy of brain tumors. *J Synchrotron Radiat* 2012;19:478-482.
30. Blanchette M, Tremblay L, Lepage M, et al. Impact of drug size on brain tumor and brain parenchyma delivery after a blood-brain barrier disruption. *J Cereb Blood Flow Metab* 2014;34:820-826.
31. Bouchet A, Bidart M, Miladi I, et al. Characterization of the 9L gliosarcoma implanted in the Fischer rat: An orthotopic model for a grade IV brain tumor. *Tumour Biol* 2014;35:6221-6233.
32. Crosbie JC, Fournier P, Bartzsch S, et al. Energy spectra considerations for synchrotron radiotherapy trials on the ID17 bio-medical beamline at the European Synchrotron Radiation Facility. *J Synchrotron Radiat* 2015;22:1035-1041.
33. Martinez-Rovira I, Sempau J, Prezado Y, et al. Monte Carlo-based treatment planning system calculation engine for microbeam radiation therapy. *Med. Phys.* 2012;39:2829-2838.
34. Coquery N, Francois O, Lemasson B, et al. Microvascular MRI and unsupervised clustering yields histology-resembling images in two rat models of glioma. *J Cereb Blood Flow Metab* 2014;34:1354-1362.
35. Brossard C, Montigon O, Boux F, et al. MP3: Medical software for processing multi-parametric images pipelines. *Front Neuroinform* 2020;14:53.
36. Lemasson B, Serduc R, Maisin C, et al. Monitoring blood-brain barrier status in a rat model of glioma receiving therapy: Dual injection of low-molecular-weight and macromolecular MR contrast media. *Radiology* 2010;257:342-352.
37. Sabatasso S, Fernandez-Palomo C, Hlushchuk R, et al. Transient and efficient vascular permeability window for adjuvant drug delivery triggered by microbeam radiation. *Cancers (Basel)* 2021;13:2103.
38. Eling L, Bouchet A, Ocadiz A, et al. Unexpected benefits of multiport synchrotron microbeam radiation therapy for brain tumors. *Cancers (Basel)* 2021;13:1-16.
39. Baselet B, Sonveaux P, Baatout S, et al. Pathological effects of ionizing radiation: Endothelial activation and dysfunction. *Cell Mol Life Sci* 2019;76:699-728.
40. Bouchet A, Lemasson B, Christen T, et al. Synchrotron microbeam radiation therapy induces hypoxia in intracerebral gliosarcoma but not in the normal brain. *Radiother Oncol* 2013;108:143-148.
41. Parrish KE, Sarkaria JN, Elmquist WF. Improving drug delivery to primary and metastatic brain tumors: Strategies to overcome the blood −brain barrier. *Clin Pharmacol Ther* 2015;97:336-346.
42. DrugBank Online. Irinotecan. https://go.drugbank.com/drugs/DB00762R. Accessed March 22, 2023.
43. Anon. Temozolomide | C6H6N6O2 - PubChem. https://pubchem.ncbi.nlm.nih.gov/compound/Temozolomide. Accessed March 13, 2024.
44. Stupp R, Hegi ME, Masonet WP, et al. Effects of radiotherapy with concomitant and adjuvant temozolomide versus radiotherapy alone on survival in glioblastoma in a randomised phase III study: 5-year analysis of the EORTC-NCIC trial. *Lancet Oncol* 2009;10:459-466.
45. Boumendjel A, McLeer-Forin A, Champelovier P, et al. A novel chalcone derivative which acts as a microtubule depolymerising agent and an inhibitor of P-gp and BCRP in in-vitro and in-vivo glioblastoma models. *BMC Cancer* 2009;9 242.
46. DrugBank Online. Meloxicam. https://go.drugbank.com/drugs/DB00814. Accessed June 26, 2023.
47. Bouchet A, Le Clec'h C, Rogalev L, et al. Meloxicam can potentiate the therapeutic effects of synchrotron microbeam radiation therapy on high-grade glioma bearing rats. *Radiat Res* 2022;197:655-661.